

NEVIS CYCLOTRON LABORATORIES

COLUMBIA UNIVERSITY
PHYSICS DEPARTMENT
Irvington-on-Hudson,
New York

Joint ONR - AEC Program
Office of Naval Research Contract
Contract N6-ori-110 Task No. 1

NEVIS - 1
R-71

SCATTERING OF 65 MEV PIONS IN HYDROGEN

D. Bodansky, A. M. Sachs
and J. Steinberger

Nevis Cyclotron Laboratories
Columbia University
Physics Department
Irvington-on-Hudson,
New York

Joint ONR - AEC Program
Office of Naval Research Contract
Contract N6-ori-110 Task No. 1

Scattering of 65 Mev Pions in Hydrogen*

D. Bodansky, A. M. Sachs and J. Steinberger
Columbia University, New York, New York

November, 1953

ABSTRACT

A measurement has been made at approximately 65 Mev of the differential cross sections in the processes $\pi^+ + P \rightarrow \pi^+ + P$, $\pi^- + P \rightarrow \pi^- + P$ and $\pi^- + P \rightarrow \pi^0 + N$ using a liquid hydrogen target and scintillation counter detectors. The measured cross sections in the center of mass are:

$\pi^+ + P \rightarrow \pi^+ + P$ (58 Mev)		$\pi^- + P \rightarrow \pi^- + P$ (65 Mev)	
θ	$\frac{d\sigma}{d\Omega}$ (mb)	θ	$\frac{d\sigma}{d\Omega}$ (mb)
36	0.24 ± 0.11	42	0.91 ± 0.13
47	0.48 ± 0.08	53	0.51 ± 0.08
64	0.66 ± 0.06	70	0.29 ± 0.06
101	1.24 ± 0.07	101	0.23 ± 0.06
129	2.10 ± 0.11	151	-0.01 ± 0.11
155	2.79 ± 0.15		

$$\frac{d\sigma}{d\Omega}(\pi^- \rightarrow \pi^0) = \left[0.96 \pm 0.03 - (1.38 \pm 0.09)\cos\theta + (0.14 \pm 0.24)\frac{3\cos^2\theta - 1}{2}\right](1 \pm 0.10) \qquad \text{(at 65 Mev)}$$

Because of coulomb interference effects, the experiment, in principle, affords the opportunity of determining the signs as well as the magnitudes of the phase shifts in an analysis including only s- and

p-waves. It is found that two very markedly different sets of phase shifts fit the data. Each of these sets includes subsets of the Fermi and Yang type. The results of this experiment, in conjunction with those of similar experiments, somewhat favor a set characterized by a strong attractive p-wave interaction in the $T = 3/2$ isotopic spin state.

I. INTRODUCTION

The angular distribution in the three scattering processes $\pi^+ + P \rightarrow \pi^+ + P$, $\pi^- + P \rightarrow \pi^- + P$, and $\pi^- + P \rightarrow \pi^0 + N$, has been studied by Anderson, Fermi, Martin and Nagle[1] at 120 and 135 Mev. The information has been extended to lower energy by several groups,[1,6] chiefly for positive pions. We present here a rather detailed study of the three processes at approximately 65 Mev. The experimental results for the $\pi^+ \rightarrow \pi^+$ reaction have been reported in brief.[7]

The results of the Chicago group were analyzed in terms of s- and p-wave scattering in the charge independent theory.[1] The reported phase shifts are, however, indeterminate with respect to a simultaneous reversal of the signs of all phase shifts. This ambiguity may, in principle, be removed by extending the study of the scattering to angles for which the coulomb amplitude is of the same order of magnitude as the nuclear amplitude. This encounters experimental difficulties at high energies, because the angles of prominent coulomb interference are small and the background from coulomb and diffraction scattering in the beam defining system and hydrogen container is then large. The situation is more favorable at lower energies, because small nuclear and larger coulomb amplitudes both act to increase the angles at which the interference is appreciable. At 65 Mev, for example, the total cross section for positive pions is 30 mb, compared to approximately 90 mb at 120 Mev, while the differential cross section at 30° is 0.14 mb per steradian

at 65 Mev compared to 0.06 mb per steradian at 120 Mev.

In this experiment, therefore, the effects of the coulomb field are quite large. Nevertheless, we find it possible to fit the experimental results with two sets of phase shifts differing in sign, but the magnitudes in one set differ considerably from those in the other. It may be possible to remove the ambiguity in sign by arguments as to magnitude. In the last section of this report we discuss an attempt to select one set by extrapolating the results at other energies.

II. EXPERIMENTAL ARRANGEMENT

A. Meson Beams

The positive meson scattering experiment was performed in the meson beam of lowest energy at the Columbia Nevis Cyclotron. The mesons are produced at an internal beryllium target, are analyzed in the fringing field of the cyclotron magnet, and emerge through a channel in the 8-foot iron shielding.

For negative meson scattering, an attempt was made to use the corresponding beam obtained by reversing the current in the cyclotron magnet. The negative mesons are, however, accompanied by a large number of electrons, probably due to the production of neutral mesons and conversion in the target of the resultant γ-rays. The dependence of this contamination on meson sign is then related to the fact that the collimated negative particles are emitted in the forward direction and the positive particles in the backward direction with respect to the proton beam. In the region of interest the number of conversion

electrons is a rapidly decreasing function of electron momentum. It is therefore possible to reduce this contamination by using a meson beam of higher energy and then decreasing the energy with absorbers.

Each beam is further analyzed in a double-focussing magnet (Fig. 1). The mesons are bent through 30°, and a parallel, monochromatic beam is focussed in both planes at a distance of 10 feet from the magnet. The beam is defined in the scintillation counter 1-2 telescope. In the case of the negative meson scattering, an absorber of 4" of lithium hydride (density = 0.5) and 1/2" of carbon is inserted before the first counter to reduce the beam energy without excessive coulomb scattering. In the position of Fig. 1 the absorber reduces the intensity by 30 percent. If the absorber, instead, is placed between the shielding and the analyzing magnet, the intensity is reduced to less than 1/10.

B. Liquid Hydrogen Target

The liquid hydrogen scatterer[8] is contained in the 3.1" diameter cylindrical cup of the metal dewar shown in Fig. 2. The target cup, made from stainless steel tubing turned to 0.004"-wall thickness, is soldered to the bottom of the larger liquid hydrogen reservoir. The hydrogen in the reservoir can be admitted to the target cup by means of a standpipe of thin wall tubing extending to the bottom of the cup. It may be returned by increasing the pressure in the cup relative to that in the reservoir. This is accomplished by closing the cup exhaust and heating a resistance element at the bottom of the cup (not shown).

The hydrogen reservoir is surrounded by a container of liquid

nitrogen which serves as a radiation shield. The target cup itself is shielded by a foil of 0.001" aluminum fastened to the bottom of the nitrogen reservoir. The design of the vacuum chamber surrounding the cup represents a compromise between conflicting requirements. In particular, it is desirable to be able to place the defining telescope near the cup, to be able to detect particles over a wide angular region, and to have the walls of the chamber as thin as possible to minimize pion scattering and γ-ray conversion. The thin wall of the vacuum chamber is a U-shaped aluminum foil, 3-3/4" high and 0.007" thick. The cup may be viewed through the thin window over an angle of 300° (see Fig. 2).

The liquid levels in the cup and reservoirs are indicated on oil manometers. The hydrogen capacity of the reservoir is 4 liters; the rate of loss is approximately 0.1 liter per hour.

C. Counters

The two stilbene crystals defining the incident beam are each viewed from the side by two 1P21 photomultipliers. Counter 1 is 3-1/4" x 2-1/2" x 1/8". Counter 2 is 2-1/4" x 2-3/4" x 1/16", and is located as close to the target as possible to insure that most of the incident beam enters the hydrogen. Counter 2 is thin to minimize the diffraction scattering from the crystal, since this contributes strongly to the background at small angles.

The scattered particles are detected in the larger liquid scintillation counters 3 and 4. In $\pi^+ \rightarrow \pi^+$ and $\pi^- \rightarrow \pi^-$ scattering, the mesons are detected in two counters, 4" x 8" x 1", illustrated in Fig. 3. The scintillating liquid, phenylcyclohexane with

terphenyl and diphenylhexatriene, is held in a lucite container. The lucite fits into a metal frame, with aluminum foil covering the faces, and with iron shields to hold 1P21 phototubes at each of the four corners. The light collection is poor compared to that in the smaller counters, and this is probably responsible for the rather low detection efficiency (~ 95 percent for the 2-counter telescope; see Section V). On the other hand, for a given angular resolution the large size (in comparison to the size of the scatterer) and rectangular shape of the counters result in a larger counting rate than would be obtained with smaller or circular counters.

In the charge-exchange scattering, single γ-rays are detected in the telescope shown in Fig. 4. The γ-rays are converted primarily in the 1/4" lead. Counter 3 is a 4-1/2"-diameter circular liquid counter, viewed from the side by three 1P21 photomultipliers. Counter 4 is large in order to accept electrons scattered in the converter. It is 8" in diameter, liquid-filled, and viewed from the back by 4 1P21's.[9] The beryllium and polyethylene absorbers are placed in front of the converter in order to stop ionizing particles. The absorber between counters 3 and 4 is intended to stop protons from low energy neutron interactions in either counter.

D. Electronics

A block diagram of the electronics is shown in Fig. 5. Signals are taken in parallel from the phototubes of each counter and fed into Hewlett Packard wide-band amplifiers. Coincidences are made between pairs of the amplified signals in diode bridge circuits with a resolving time of 10^{-8} sec. The coincidence signals are then amplified

to a level of approximately 10 volts, discriminated in a diode circuit, and then formed to uniform negative pulses 5×10^{-8} sec long and 15 volts high. The dead time of the pulse former is $\sim 10^{-7}$ sec.[10] The outputs are again paired in diode coincidence circuits, as shown in Fig. 5. The 1-2 pulse is scaled in a system with 10^{-7} sec dead time.[11] All other circuits are commercially available through the Atomic Instrument Company. Inspection of the block diagram shows that the resolving time for accidental coincidences between 1-2 counts and 3-4 counts is just that of the 1-3 coincidence, $\sim 10^{-8}$ sec. Several intermediate coincidence rates are scaled to check the operation of the equipment, but the pertinent data are the over-all quadruple counts and the 1-2 counts.

III. CALIBRATION MEASUREMENTS

A. Beam Energy

The integral range distributions of the two beams were determined by placing counter 3 in line with counters 1 and 2, ~12" behind counter 2, and measuring the ratio of rates 1-2-3 and 1-2 as a function of the thickness of carbon absorber placed in front of counter 3. The results are given in Fig. 6 for the positive and negative meson beams. Each of these curves exhibits the characteristic initial slope due to nuclear interactions of the pions and a sharp drop as the pions reach the end of their range in the absorbers. A second drop occurs at a higher range corresponding to μ-mesons with the same momentum. The remainder of the beam is attributed to electrons.

Using Aron's tabulation[12] of the range-energy relationships, the

mean energy of the pions at the center of the target is determined to be 58 Mev for the positive and 65 Mev for the negative mesons. The half-width of the energy distribution at half-maximum is estimated to be 3 Mev for the positive mesons and 5 Mev for the negative mesons and is due to the initial beam spread, ionization loss in the target, and the effect of the absorbers in the negative beam.

B. Angular Resolution

By rotating the detecting telescope through the forward angles, curves like the one shown in Fig. 7 are obtained for each geometry in the $\pi^+ \rightarrow \pi^+$ and $\pi^- \rightarrow \pi^-$ scattering. These curves are a measure of the angular resolution; their centers determine the positions $\theta = 0^\circ$. For $\pi^+ \rightarrow \pi^+$ scattering, the half-width at half-maximum is 7° for L = 18.5" and 5° for L = 27.5" where L is the distance from the center of the target to counter 4. For $\pi^- \rightarrow \pi^-$ scattering, where L = 15.5", it is 11°.

IV. EXPERIMENTAL RESULTS

The experimental results are presented in Table I. Counting rates were obtained at each angle alternately with the hydrogen cup full and empty. After each such set the detecting telescope was turned to $\theta = 0^\circ$ to check the stability of the equipment.

Table I. Experimental Data

	θ_{lab} (deg)	L (inches)	Counts from Hydrogen per 10^6 Incident Particles	Ratio of Counts from Hydrogen to Background	Carbon Absorber (gm/cm^2)
$\pi^+ \rightarrow \pi^+$	30	32.5	1.5 ± 1.6	.02	0
		27.5	2.1 ∓ 1.4	.04	4.4
	40	27.5	5.2 ± 0.8	.19	0
		18.5	4.2 ∓ 4.8	.05	0
	55	27.5	4.5 ± 1.6	.26	0
		18.5	14.0 ∓ 1.3	.47	0
	90	27.5	11.5 ± 1.2	1.96	0
		18.5	20.4 ∓ 1.1	1.11	0
	120	27.5	11.9 ± 1.4	1.44	0
		18.5	30.5 ∓ 1.6	1.36	0
	150	27.5	12.0 ± 1.5	1.04	0
		18.5	32.2 ∓ 1.5	.92	0
$\pi^- \rightarrow \pi^-$	35	15.5	29.4 ± 3.8	.10	4.4
	45	15.5	16.7 ± 2.3	.13	4.4
	60	15.5	10.1 ± 1.3	.23	4.4
	90	15.5	8.0 ± 1.0	.26	2.2
	145	15.5	3.6 ± 1.3	.06	0
$\pi^- \rightarrow \gamma$	45	11	7.6 ± 0.6	.68	
	90	11	15.2 ± 0.6	2.53	
	145	11	20.2 ± 1.5	1.75	
		14	12.1 ∓ 0.9	1.12	

The difference counting rates are given with their statistical probable errors. The distance L is measured from the center of the hydrogen cup to the center of counter 4 for the elastic scattering and to the front of counter 3 for the charge exchange scattering

measurements. In some measurements, carbon absorber was placed in front of counter 4 to reduce the background from short-range particles. The thickness of the absorber is indicated in the last column.

With average cyclotron conditions, 10^6 particles passed through the defining telescope in about 10 minutes for both the positive and negative beams. With this intensity, approximately 110 hours of operation were required to make the measurements listed in Table I.

V. CALCULATION OF CROSS SECTIONS

The differential cross sections in the laboratory system are calculated using the relation

$$\frac{d\sigma'}{d\Omega} = \frac{10^{-6}\, n}{NoA^{-1} t\, \rho (1-a) \epsilon \Omega} \qquad (1)$$

where $\frac{d\sigma'}{d\Omega}$ = uncorrected differential cross section

n = counting rate per 10^6 incident particles

No = Avagadro's number

A = atomic weight of hydrogen

t = average thickness of hydrogen target (gm/cm^2)

ρ = fraction of incident particles which are π mesons

a = attenuation of scattered mesons due to nuclear absorption

ϵ = efficiency of detector telescope

Ω = solid angle of detector telescope

The counting rates, n, are obtained from Table I. The values used for the other relevant quantities are listed in Table II and are discussed below.

Table II. Experimental parameters

	$\pi^+ \rightarrow \pi^+$	$\pi^- \rightarrow \pi^-$	$\pi^- \rightarrow \gamma$
t (gm/cm^2)	0.460	0.440	0.440
ρ	0.89	0.78	0.78
α 0 gm/cm^2 of C	0.03	0.03	
2.2 gm/cm^2 of C		0.06	
4.4 gm/cm^2 of C	0.08	0.08	
Ω L = 15.5"		0.123	
L = 18.5"	0.0860		
L = 27.5"	0.0389		
L = 32.5"	0.0229		
ϵ	0.91	0.97	
$(\epsilon\Omega)_1$ L = 11"			0.0357*
L = 14"			0.0220*

* for γ-rays from stopped mesons

A. Target Thickness

In order to determine the average thickness of the liquid hydrogen in the path of the mesons counted in the incident telescope, the lateral extension of the positive and negative beams was scanned with a 1/8"-wide crystal directly behind the target. The experimental curve taken in the positive beam is shown in Fig. 8. By extrapolating this curve to the center of the hydrogen cup and folding t into a 3.1"-diameter circle (the horizontal cross section of the cup), the relevant weighted average of the distance through the cup is obtained. The net thickness, t, of the liquid hydrogen minus that of gas remaining in the cup when the liquid is removed is 0.460 gm/cm^2 for the positive and 0.440 gm/cm^2 for the negative beam.

B. Beam Purity

The composition of the incident beam is determined from the range curves of Fig. 6. The μ-mesons and electrons, which are assumed to undergo negligible scattering in hydrogen, are estimated to comprise 11 percent of the positive and 22 percent of the negative beam. The remainder consists of pions.

C. Nuclear Attenuation

A fraction, α, of the scattered mesons will not be counted by the detection telescope due to interactions in counter 3 and in the carbon absorbers which were at times placed in front of counter 4. Counter 3 contains 2.2 gm/cm^2 of carbon. The values listed in Table II are calculated using a mean free path in carbon of 80 gm/cm^2 for the loss of mesons from the detecting system.[13]

D. Solid Angle and Efficiency - - Elastic Scattering

In the elastic scattering measurements the solid angle, Ω, is defined by counter 4. It is estimated that, on the average, a meson must penetrate 1/4" into counter 4 to be detected, and therefore the appropriate distance in calculating the solid angle is L - 1/4". A small correction is made to account for the fact that the average distance from the target to the counter is greater than the distance along the central axis. The solid angles calculated from these considerations are listed in Table II.

The efficiency, ϵ, of the detecting telescope for counting charged mesons is measured by placing the larger counters 3 and 4 between counters 1 and 2, and finding the ratio of over-all quadruple coincidences to 1-2 coincidences. For positive mesons this ratio is

found to be 0.91, while for negative mesons it is 0.97. The improvement in the latter case is believed due to a change of phototubes.

E. Solid Angle and Efficiency - - Charge Exchange Scattering

In order to maximize the efficiency for gamma rays, a lead converter is used which is 1/4" thick (1.2 radiation lengths) and covers the area of counter 3. As a consequence, the complications of multiple processes and scattering of the resulting electrons prevent a simple and accurate calculation of the efficiency or solid angle. In fact, the quantities ϵ and Ω cannot here be independently defined. It is therefore advantageous to determine experimentally the product $\epsilon\Omega$.

The calibration of $\epsilon\Omega$ is obtained by comparing the counting rate of the normal system with that in a detection system for which the efficiency can be calculated rather accurately. γ-rays from negative pions stopped in hydrogen are used in the comparison, providing a high flux with known energy distribution.[14] Absorbers are therefore placed in the incident beam and the resulting γ-rays are detected in three different geometries: (1) the system normally used (see Fig. 4); (2) the same geometry with the exception that the absorbers and converter are replaced by a thin lead converter, 0.97 gm/cm^2 thick and 4" in diameter, directly in front of counter 3; (3) the same geometry as in (2), but with the thin lead converter replaced by a polyethylene absorber in which ionization losses are the same. Counting rates for the events from hydrogen are $N_1 = 764 \pm 12$, $N_2 = 296 \pm 6$ and $N_3 = 160 \pm 5$ per 10^6 incident particles. In addition, we require the efficiency of the 3-4 telescope for counting electron pairs. The

efficiency for counting mesons is found to be 84 percent by the method used in the elastic scattering experiments. In most cases two electrons pass through the telescope for each γ-ray converted in the thin lead. Their combined ionization loss is slightly greater than that of a 65-Mev meson and the efficiency for pair detection may be somewhat higher than the measured meson efficiency. This possible difference is neglected.

For the normal system,

$$(\epsilon\Omega)_1 = \frac{N_1}{N_2-N_3}\left[(\epsilon\Omega)_2 - (\epsilon\Omega)_3\right]$$

The difference $(\epsilon\Omega)_2 - (\epsilon\Omega)_3$ can be calculated with the help of the γ-ray conversion cross sections of Lawson[15] and Dewire, Ashkin and Beach.[16] With thin converters, multiple processes can be neglected and, in the geometry used, scattering corrections are unnecessary. For the γ-rays from stopped mesons, the effective mean free path in lead is 11.4 gm/cm^2, corresponding to a conversion efficiency of 0.082 in the thin lead converter. The conversion efficiency of the polyethylene is calculated to be 0.007. Therefore, for L = 11 inches, $(\epsilon\Omega)_2 - (\epsilon\Omega)_3 = 0.00655$ and $(\epsilon\Omega)_1 = 0.0368$ steradians.

This efficiency, together with the corresponding value for L = 14 inches, is listed in Table II. The values include an additional small correction, $3 \pm 2\%$, for the effects of γ-ray conversion in the heavy members of the target. These values are for the γ-rays from stopped mesons and must be adjusted to account for the different energies in the scattering experiment.

The quantities in Table II, other than the γ-ray efficiency-solid

angle products, are believed to be sufficiently well known that errors in their determination do not contribute significantly to the errors in the determination of the cross sections. The γ-ray products $(\epsilon \Omega)_1$ have three principle sources of error: (1) A statistical probable error of 6 percent due to errors in the counting rates N_1, N_2 and N_3; (2) An uncertainty in the efficiency for pair detection which is estimated to be + 5 to -3 percent; (3) The 2 percent uncertainty in the correction for electrons converted in the heavy parts of the target. The over-all probable error in the products $(\epsilon \Omega)_1$ is therefore about $\pm$ 10 percent.

F. Corrections

Several corrections are applied to the cross sections calculated from Equation (1). Correction 1 is applied to the $\pi^+ \rightarrow \pi^+$ cross sections at all angles in an attempt to correct for the decrease in background counts when hydrogen is in the cup. One would like to assume in a subtraction procedure that the background is unaffected by the presence of the target - - in this case the liquid hydrogen. This is not always justifiable. For instance, a meson star in the wall of the target cup could have a proton prong which will be detected if the cup is empty but, due to additional ionization loss in the hydrogen, will not be detected if the cup is full. Inelastic meson scattering can give rise to similar events. An attempt to set an upper limit on this effect was made by comparing the background counting rates with different amounts of carbon absorber in the path of the background particles. It was found on this basis that if half of the background traverses the entire cup, then the measured

laboratory differential cross sections decrease by about 0.12 mb. This is probably an overestimate of the effect as some of the background does not arise in the walls of the cup. Therefore a small correction of 0.08 $\pm$ 0.06 mb/steradian is added to the cross sections. In the $\pi^- \rightarrow \pi^-$ scattering the same problem exists, but to a smaller extent, since the number of protons from negative meson stars is considerably less than from positive meson stars. The correction is expected to be small and, since it requires untested assumptions about the nature of the background, no similar correction is made.

Correction 2 is applied to the $\pi^- \rightarrow \gamma$ cross sections to account for the γ-rays from the radiative capture of the meson. The cross section for this process is calculated from that of the inverse process, which is taken to be equal[17] to the cross section for the process $\gamma + P \rightarrow \pi^+ + N$.[18] The correction is 0.06 mb/steradian.

Correction 3 is applied to the $\pi^- \rightarrow \pi^-$ cross sections to account for the detection of converted γ-rays. 1.1 percent of the γ-rays produced in charge exchange scattering are internally converted in the hydrogen[8,19] and an additional 2.4 percent are converted in passing through the target. An approximate calculation indicates that electrons from γ-rays converted in the heavy brass parts of the target contribute an additional flux in the detecting telescope equal to 2.5 $\pm$ 1.5 percent of the γ-ray flux. Thus at each angle we subtract from the observed $\pi^- \rightarrow \pi^-$ cross section 0.06 $\pm$ 0.02 of the $\pi^- \rightarrow \gamma$ cross section.

Correction 4 is applied only to the 150° point in the $\pi^+ \rightarrow \pi^+$ scattering. Mesons detected in the backward direction have about

one-half the energy of the incident mesons. In the arrangement used, those mesons which traverse most of the hydrogen target, are then scattered at 150°, and have to pass again through most of the target before reaching the telescope, may have insufficient range to be counted. The correction for this effect required the addition of 10 ± 5 percent to the measured cross section at 150°. No similar correction is required in the $\pi^- \rightarrow \pi^-$ scattering, as the incident meson energy is greater.

G. Calculated Cross Sections

The laboratory cross sections for the elastic scattering processes, as calculated from Equation (1) and including the corrections discussed above, are presented in Table III. The corresponding center of mass angles and cross sections are also given. The errors include only the probable statistical errors and the probable errors in the corrections. Other uncertainties are thought to be small.

Table III. Differential Cross Sections

	Laboratory system		Center of mass system	
	θ (deg)	$\frac{d\sigma}{d\Omega}$ (mb/ster)	θ (deg)	$\frac{d\sigma}{d\Omega}$ (mb/ster)
$\pi^+ \rightarrow \pi^+$	30	0.33 ± 0.15	36	0.24 ± 0.11
58 Mev	40	0.64 ± 0.10	47	0.48 ± 0.08
	55	0.81 ± 0.08	64	0.66 ± 0.06
	90	1.21 ± 0.06	101	1.24 ± 0.07
	120	1.68 ± 0.09	129	2.10 ± 0.11
	150	1.95 ± 0.10	155	2.79 ± 0.15
$\pi^- \rightarrow \pi^-$	35	1.24 ± 0.17	42	0.91 ± 0.13
65 Mev	45	0.66 ± 0.10	53	0.51 ± 0.08
	60	0.35 ± 0.07	70	0.29 ± 0.06
	90	0.22 ± 0.06	101	0.23 ± 0.06
	145	-0.01 ± 0.07	151	-0.01 ± 0.11

In the charge exchange scattering the neutral pion distribution is related to the γ-ray counting rate, $n(\theta)$, by

$$n(\theta) = Cq(\theta) \int \frac{d\sigma(\theta')}{d\Omega'} \quad W(\alpha) \quad \epsilon\Omega(E)d\Omega' \qquad (2)$$

where $C = 10^{-6}/N\sigma A^{-1}t\rho$

$$q(\theta) = \left(\frac{d\sigma}{d\Omega}\right)_{lab} \Big/ \left(\frac{d\sigma}{d\Omega}\right)_{c.\ of\ m.} = (1-\beta_o^2)/(1-\beta_o\cos\theta)^2$$

$\frac{d\sigma(\theta')}{d\Omega'}$ = π^o differential cross section in the center of mass system

$W(\alpha)$ = probability that a π^o emits a γ-ray at an angle $\alpha = (1-\beta^2)/2\pi(1-\beta\cos\alpha)^2$

$E(\theta,\alpha)$ = γ-ray energy in the laboratory system

$$= \frac{m_{\gamma o}c^2}{2}\sqrt{\frac{1-\beta^2}{1-\beta_o^2}}\;\frac{1+\beta\cos\theta}{1-\beta\cos\alpha}$$

θ = angle of detected γ ray in the laboratory system

θ' = π^o angle in the center of mass system

α = angle between π^o and γ-ray in the center of mass system

βc = velocity of π^o in the center of mass system

$\beta_o c$ = velocity of center of mass.

To integrate Equation (2) we use an expansion in Legendre polynominals similar to that of Anderson, Fermi, Martin and Nagle,[1] but with the explicit consideration of the variation with energy of γ-ray detection efficiency. If pion scattering occurs only in the s- and p-states (see Section VI), the cross section can be expressed as

$$\frac{d\sigma(\theta')}{d\Omega'} = \sum_{\lambda=0}^{2} \sigma_\lambda P_\lambda(\cos\theta').$$

Similarly, $W(\alpha)\,\Omega(\theta,\alpha) = \sum \omega_\lambda(\theta) P_\lambda(\cos\alpha)$.

Then $$n(\theta) = 4\pi C q(\theta) \sum_{\lambda=0}^{2} (2\lambda+1)^{-1}\,\sigma_\lambda \omega_\lambda(\theta) P_\lambda(\cos\theta''), \quad (3)$$

where θ = γ ray angle in the center of mass system. The counting rates $n(\theta)$ listed in Table IV, are obtained from Table I using Correction 2 for the γ-rays from the process $\pi^- + P \rightarrow \gamma + N$.

Table IV. Corrected γ-ray counting rates
n(θ) and correlation coefficients $\omega_\ell(\theta)$

Lab. angle θ	n(θ)	Correlation coefficients $\omega_\ell(\theta)$ $\ell = 0$	$\ell = 1$	$\ell = 2$
45°	7.0 ± 0.8	5.76×10^{-3}	11.12×10^{-3}	9.54×10^{-3}
90°	14.6 ± 0.9	5.46	10.83	9.40
145°	19.3 ± 1.6	5.12	10.49	9.18

The coefficients $\omega_\ell(\theta)$ are

$$\omega_\ell(\theta) = 1/2\ (2\ell+1) \int_0^\pi W(\alpha)\, \epsilon\Omega(\theta,\alpha)\, P_\ell(\cos\alpha)\sin\alpha\, d\alpha\,. \quad (4)$$

To evaluate the coefficients we must determine $\epsilon\,\Omega\,(\theta,\alpha)$, i.e., determine the energy dependence of the efficiency. Silverman and Cosmoni[20] have found in a similar telescope that the detection efficiency may be represented by

$$\epsilon = \text{const}\ x(1-e^{-(E-25)/40}), \quad (5)$$

where E is in Mev. Ignoring the slight difference in geometry, we assume the same energy dependence but determine the constant from the measured value of $(\epsilon\Omega)_1$ for γ-rays from stopped mesons. Using the known energy spectrum of these γ-rays[14] the proportionality constant for $\epsilon\,\Omega$ is calculated to be 0.0471 steradian.

Inspection of (5) shows that the detection efficiency is an increasing function of γ-ray energy, and its inclusion in (4) has the effect of favoring the detection of γ-rays with small correlation angles α. The correlation between γ-ray and π^0 is therefore some-

what better than would be obtained with a detection system of uniform efficiency. If the energy dependence of $\epsilon\Omega$ is replaced by some average value, at best chosen to give the same total cross section, the correlation coefficients ω_0 remain essentially the same, but ω_1 is depressed approximately by the factor 1.3 and ω_2 by 1.5.

Equation (4) is integrated numerically and the resulting coefficients are listed in Table IV. Equation (3) is evaluated at the three experimental angles θ. We find $\sigma_0 = 0.96 \pm 0.03$ mb/ster, $\sigma_1 = -1.38 \pm 0.09$ mb/ster, $\sigma_2 = 0.14 \pm 0.24$ mb/ster. The errors correspond to the statistical probable errors in $n(\theta)$. The previously discussed 10 percent uncertainty in detection efficiency is not included. The error due to possible inadequacy of the assumed energy dependence of the efficiency is believed to be small, since the calibration is performed at an intermediate energy. We therefore find for the center of mass system

$$\frac{d\sigma(\theta)}{d\Omega}(\pi^- \rightarrow \pi^0) = (1\pm0.10)\left[0.96\pm0.03 - (1.38\pm0.09)\cos\theta + (0.14\pm0.24)\left(\frac{3\cos^2\theta-1}{2}\right)\right]$$

The corresponding center of mass γ-ray cross section is

$$\frac{d\sigma(\theta)}{d\Omega}(\pi^- \rightarrow \gamma) = (1\pm0.10)\left[1.98\pm0.06 - (1.41\pm0.09)\cos\theta + (0.07\pm0.11)\left(\frac{3\cos^2\theta-1}{2}\right)\right].$$

VI. PHASE SHIFT ANALYSIS

We have attempted to express the experimental results in terms of phase shifts. Following the Chicago group,[1] the analysis is performed assuming (a) that the meson-nucleon coupling is charge-independent,

and (b) only s- and p-states scatter appreciably. There is a growing body of evidence[21] to support (a), chiefly the experiments on nucleon-nucleon meson production,[22] the level structure of isobaric nuclei,[23] and perhaps also the success of the assumption in this and preceding experiments.[1] In support of (b) we note that in this experiment the meson momentum is 0.88 $m_\pi c$, and if the meson-nucleon interaction has a range not in excess of the meson Compton wavelength ($\sim 1.4 \times 10^{-13}$cm) the scattering in higher angular momentum states may be expected to be small. Nevertheless, appreciable d-scattering, even at this low energy, is entirely possible. The experiment does not permit the determination of the relative importance of higher orbital states. On the other hand, the pronounced asymmetries about 90° do make it necessary to combine at least one even and one odd state.

In the analysis of the higher energy experiments the magnitudes of the phase shifts were determined, but an ambiguity remained which permitted the simultaneous reversal of the signs of all phase shifts. This ambiguity may, in principle, be removed by studying the scattering in situations in which the coulomb interference enters significantly, since the coulomb amplitudes are known. At the smallest angles of this experiment the coulomb amplitudes are of the same order of magnitude as the observed amplitudes and therefore affect the scattering strongly.

An analysis of pion-nucleon scattering with the inclusion of coulomb effects has been made by Van Hove.[24] For the present purposes it is necessary to retain only first order coulomb terms and to consider the phase shifts small. In this approximation the cross

sections are:

$$\frac{d\sigma}{d\Omega} = \lambda^2 \left\{ \left[\sum_{t=1/2}^{3/2} \xi^t \left(\frac{\alpha}{2\sin^2(\theta/2)} \right) + X^t + Y^t \cos\theta \right]^2 + \left[\left(\sum_{t=1/2}^{3/2} \xi^t Z^t \right)^2 \sin^2\theta \right] \right\} \qquad (6)$$

where $X^t = \delta(s^t)$

$Y^t = 2\delta(P^t_{3/2}) + \delta(P^t_{1/2})$

$Z^t = \delta(P^t_{3/2}) - \delta(P^t_{1/2})$

for $\pi^+ \rightarrow \pi^+$: $\xi^{1/2} = 0$, $\xi^{3/2} = 1$, $\alpha = -e^2/\hbar v$

$\pi^- \rightarrow \pi^-$: $\xi^{1/2} = 2/3$, $\xi^{3/2} = 1/3$, $\alpha = +e^2/\hbar v$

$\pi^- \rightarrow \pi^0$: $\xi^{1/2} = -\sqrt{2}/3$, $\xi^{3/2} = \sqrt{2}/3$ $\alpha = 0$

$\lambda\!\!\!^{-} = (2\pi)^{-1}$ x wavelength in center of mass

The precise determination of v in the coulomb term requires solution of the relativistic two-body problem, but according to Van Hove the relative velocity in the center of mass may be expected to be nearly correct.

The degree of agreement between the observed cross sections and calculated ones can be quantitatively expressed in terms of $\omega = \sum_{i=1}^{14} \left(\frac{\Delta_i}{PE_i} \right)^2$ where Δ_i is the difference between the observed and calculated cross sections at the i^{th} point and PE_i is the probable error of the cross section at the i^{th} point. The best fit is the one which minimizes ω, but any fit which gives a sufficiently small value of ω is an acceptable fit. The determination of the phase shifts

which give the best fit and an analysis of the possible deviation of the phase shifts from the best-fit values is difficult without the aid of computing machines. N. Mitropoulos has kindly consented to investigate this problem using the Los Alamos computer. Pending the completion of this more thorough analysis, a preliminary study has been made.

It will be noticed that the experimental cross sections are obtained at two energies, 65 and 58 Mev. The phase shifts were calculated to apply at 65 Mev, and were extrapolated for the purpose of comparison with the $\pi^+ \rightarrow \pi^+$ results at 58 Mev. In the absence of information on the energy dependence of the individual phases, we have decreased all phase shifts in proportion to the cube of the center of mass momentum, in accord with the observed energy dependence of the total cross section.

There are four sets of phase shifts which give reasonably good fits. It is believed that the data preclude sets of phase shifts radically different from these. These phase shifts are listed in Table V.[25] Sets A and B differ in the reversal of the signs of the spin-flip terms Z^t and correspond to the types first discussed by Fermi and Yang respectively.[1] For small phase shifts the Fermi and Yang solutions lead to identical cross sections and no choice can be made between them.

Table V. Phase shifts at 65 Mev.

	Phase shifts in degrees					
	$\delta(S^{3/2})$	$\delta(P^{3/2}_{1/2})$	$\delta(P^{3/2}_{3/2})$	$\delta(S^{1/2})$	$\delta(P^{1/2}_{1/2})$	$\delta(P^{1/2}_{3/2})$
Fermi type:						
Set IA	-6.2	-1.9	+9.1	+10.9	+0.4	-2.6
Set IIA	+14.5	-1.4	-2.8	-4.6	-1.3	+7.1
Yang type:						
Set IB	-6.2	+12.8	+1.7	+10.9	-3.6	-0.6
Set IIB	+14.5	-3.2	-1.9	-4.6	+9.9	+1.5

The cross sections determined by these phase shifts are compared with the experimental results in Figs. 9, 10 and 11. In the charge exchange scattering the comparison is made directly with the counting rates using Equation (3) and the σ's determined by the phase shifts: in Set I, $\sigma_0 = 0.98$, $\sigma_1 = -1.24$, $\sigma_2 = +0.29$, and in Set II, $\sigma_0 = 0.97$, $\sigma_1 = -1.31$, $\sigma_2 = 0.34$. Set I gives an appreciably better fit than Set II for the $\pi^+ \rightarrow \pi^+$ cross sections but a slightly poorer fit for the $\pi^- \rightarrow \pi^-$ and $\pi^- \rightarrow \pi^0$ cross sections. Both sets give acceptable over-all fits and are characterized by deviation parameters ω of 14 for Set I and 20 for Set II. Slight changes in the phase shifts within each set can probably lead to smaller values of ω, but a great improvement is unlikely. The fits can be judged in terms of the median deviation $\omega_{1/2}$ expected in fitting 14 experimental points in a theory with 6 free parameters. $\omega_{1/2}$ is approximately 15. It should be noted that the significance of the comparison of ω with the

expected $\omega_{1/2}$ is limited by the uncertainties in the stated errors. Thus, although Set I is the better fit, Set II is not excluded. The present measurements, considered alone, therefore do not eliminate the ambiguity in the signs of the phase shifts.

In the Fermi-type solutions, both in Set IA here and in the Chicago analysis,[1] the phase shifts $\delta(P^{1/2}_{1/2})$, $\delta(P^{1/2}_{3/2})$ and $\delta(P^{3/2}_{1/2})$ are small. Because of the possible theoretical importance we have attempted to fit the experimental results under the assumption that these phase shifts are identically zero. Such a fit is characterized by a deviation ω of the order of 50, and we consider it unlikely that our results are in error by such an amount. We therefore are of the opinion that although the interaction in these states is weak, it is non-vanishing.

The total cross section cannot be simply defined because of the small angle coulomb scattering. A measure of the nuclear contribution to the total cross section may be given by integration of Equation (6) with the coulomb term omitted. These cross sections, for the three scattering processes, are presented in Table VI with estimated probable errors.

Table VI. Total cross sections

Process	Energy (Mev)	Total Cross section (mb)
$\pi^+ \rightarrow \pi^+$	58	15.8 ± 1.5 [a]
	65	20.4 ± 2.0 [b]
$\pi^- \rightarrow \pi^-$	65	2.9 ± 0.5 [b]
$\pi^- \rightarrow \pi^0$	65	12.4 ± 1.5 [b]

[a] From phase shifts corresponding to 58 Mev $\pi^+ \rightarrow \pi^+$ scattering.

[b] From phase shifts of Table V, Set I.

VII. DISCUSSION OF RESULTS

A. T Dependence

The cross sections for positive and negative pions, σ^+ and $\sigma^- = \sigma(\pi^- \rightarrow \pi^-) + \sigma(\pi^- \rightarrow \pi^0)$, can be used to determine the cross sections in the T = 1/2 and T = 3/2 states, $\sigma^{1/2}$ and $\sigma^{3/2}$. In particular

$$\sigma^+ = \sigma^{3/2}$$
$$\sigma^- = \frac{2}{3}\ \sigma^{1/2} + \frac{1}{3}\ \sigma^{3/2}.$$

At higher energy the scattering is almost entirely in the T = 3/2 state, corresponding to the 3 to 1 ratio of the total cross sections σ^+ and σ^-. This is no longer the case at 65 Mev. The ratio of total cross sections is about 4 to 3, and this corresponds to $\sigma^{3/2} = 1.6\ \sigma^{1/2}$. In the phase shift Set I this increase in the relative importance of the T = 1/2 state is reflected in $\delta(S^{1/2})$, which is the largest single phase shift. The contributions of s- and p-wave phase shifts to $\sigma^{1/2}$ and $\sigma^{3/2}$ are given in Table VII.

Table VII. Contributions of S- and P-waves to $\sigma^{1/2}$ and $\sigma^{3/2}$ at 65 Mev for phase shifts of Sets I and II (mb)*

	Set I		Set II	
	S	P	S	P
T = 1/2	11.6	1.3	2.1	10.1
T = 3/2	3.7	16.7	20.5	1.7

* Solutions of Yang and Fermi types give same results for contributions from S- and P-states.

B. Discrimination between Set I and Set II Solutions

We have attempted to select between Sets I and II by extrapolating the phase shifts at higher and lower energies. For T = 3/2 the main difference between the two sets is that the scattering is mainly in the p-state in I and in the s-state in II. At higher energies the p-state is known to be dominant over the s-state, and if this could be shown to persist to 65 Mev, Set II would definitely be excluded. There are, however, serious difficulties in this procedure: (a) In the absence of an adequate theory on the energy dependence of meson-nucleon scattering, any extrapolation is necessarily based on questionable preconceptions; (b) the reported phase shifts are best fits to the data, but may often be seriously altered without exceeding the limits imposed by the experimental results; (c) the neglect of higher angular momentum states may be misleading.

Subject to these reservations we have assembled in Table VIII the relevant published phase shifts.

Table VIII. Published phase shifts at various energies (deg.)

Energy	40 Mev[6]	65 Mev		78 Mev[1]	120 Mev[1]	135 Mev[1]
$\frac{P}{m_\pi c}$	.68	.88		.97	1.24	1.32
		Set I	Set II			
S-wave						
$\delta(S^{3/2})$	-2	-6.2	14.5	-6	-15	-14
$\delta(S^{1/2})$		10.9	-4.6		9	10
Fermi-type P-wave						
$\delta(P^{3/2}_{3/2})$	6	9.1	-2.8	13	30	38
$\delta(P^{3/2}_{1/2})$	0.7	-1.9	-1.4	-3	4	5
$\delta(P^{1/2}_{3/2})$		-2.6	7.1		2	2
$\delta(P^{1/2}_{1/2})$		0.4	-1.3		-3	-5
Yang-type P-wave						
$\delta(P^{3/2}_{3/2})$	2.5	1.7	-1.8	2	13	17
$\delta(P^{3/2}_{1/2})$	7.8	12.8	-3.2	18	39	49
$\delta(P^{1/2}_{3/2})$		-0.6	1.8		-1	-3
$\delta(P^{1/2}_{1/2})$		-3.5	9.9		4	6

On this basis we would reject Set II because of the abruptly large s-wave and small $p_{3/2}$-wave phase shifts in the T = 3/2 state. However,

if the experimental results at other energies can be reasonably fitted with phase shifts with a large $s^{3/2}$ and small $p^{3/2}$ interaction, this rejection of Set II is impossible. A re-examination of the results at 40^{6} and 78^{1} Mev shows that it is quite possible to find such phase shifts (see Table IX).[26] We do not know if this is also possible at higher energies.

Table IX. Alternative phase shifts (Set II) in T = 3/2 state for 40, 65 and 78 Mev.

Energy in Mev	Set II Phase shifts in degrees		
	$\delta(S^{3/2})$	$\delta(P^{3/2}_{3/2})$	$\delta(P^{3/2}_{1/2})$
40	9	-2	-2
65 (Fermi type)	14.5	-2.8	-1.4
78	19	-2.5	-2.5

Other experimental results which might provide a basis for the choice between Sets I and II are the measurements of 60-Mev pion scattering in carbon by Byfield, Kessler and Lederman,[27] and of 40-Mev pion scattering in hydrogen by Perry and Angell.[6] In the carbon experiments it was found that the scattering in the forward directions corresponds to that of an attractive potential. The same conclusion is valid for both Sets I and II of the data presented here. Bethe[28] has pointed out that if the p-state interaction is dominant then it is attractive, in agreement with our Set I. Similarly, the Rochester

group have noted that if either (a) $\delta(P^{3/2}_{3/2})$ is greater than $\delta(S^{3/2})$[6] or (b) $\delta(P^{1/2}_{1/2})$, $\delta(P^{1/2}_{3/2})$ and $\delta(P^{3/2}_{1/2})$ are all very small,[29] the signs can be determined. In both cases the results correspond to Set I. However, if Set II were indeed correct these arguments would fail. Therefore, they do not provide an independent basis for selection.

If the pion-nucleon scattering were characterized by phase shifts similar to those of our Set II and Table IX, that is, by a large $S^{3/2}$ and small $p^{3/2}$ interaction, a fairly radical departure from present viewpoints would be required. However, although the experiments are not conclusive on this point, we are of the opinion that they establish a preference for Set I and the similar published phase shifts at other energies. In this case the signs of the phase shifts are determined. In particular, the most important interaction, namely that in the p-state with isotopic spin 3/2, is attractive. This is a result which should be of considerable theoretical interest, since it verifies a prediction of the pseudoscalar meson theory (with either form of the coupling).[30,31] This particular theoretical result, namely the sign of the interaction in the $p^{3/2}_{3/2}$ state, is probably insensitive to the inadequacy of the calculational methods which makes more quantitative theoretical deductions uncertain. Experimental verification of this theoretical prediction is therefore believed to be significant.

We wish to extend our thanks to Professor H. A. Boorse for the use of a hydrogen liquefaction apparatus, to Mr. E. Ihasz for the construction of the dewar, and to Mr. W. Chinowsky and H. Wolfe for assistance in the liquefaction operations.

REFERENCES

* This research was supported by the joint program of the Office of Naval Research and the Atomic Energy Commission.

1 Anderson, Fermi, Martin, and Nagle, Phys. Rev. 91, 155 (1953).

2 Fowler, Fowler, Schutt, Thorndyke, and Whittemore, Phys. Rev. 86, 1053 (1952); 91, 135 (1953).

3 G. Goldhaber, Phys. Rev. 89, 1187 (1953).

4 Minguzzi, Puppi, and Ranzi (Not as yet published. We wish to thank Prof. Puppi for a prepublication copy of this work.)

5 A. Roberts and J. Tinlot, Phys. Rev. 90, 951 (1953).

6 J. P. Perry and C. E. Angell, Phys. Rev. 91, 1289 (1953).

7 Bodansky, Sachs, and Steinberger, Phys. Rev. 90, 996 (1953); 90, 997 (1953).

8 Lindenfeld, Sachs, and Steinberger, Phys. Rev. 89, 531 (1951).

9 Durbin, Loar, and Havens, Phys. Rev. 88, 179 (1952).

10 We are indebted to V. Fitch for the design of this circuit.

11 V. Fitch, Rev. Sci. Inst. 20, 942 (1949).

12 W. A. Aron, UCRL Report 1325.

13 Isaacs, Sachs, and Steinberger, Phys. Rev. 85, 803 (1952).

14 Panofsky, Aamodt, and Hadley, Phys. Rev. 81, 565 (1951).

15 J. L. Lawson, Phys. Rev. 75, 433 (1949).

16 Dewire, Ashkin, and Beach, Phys. Rev. 83, 505 (1951).

17 The experimental evidence on the equality of the $\gamma + P$ and $\gamma + N$ photoproduction rests on the near unity ratio of π^-/π^+ photoproduction in deuterium. See e.g., White, Jacobson and Schultz, Phys. Rev. 88, 836 (1952) and Littauer and Walker, Phys. Rev. 86, 838 (1952).

REFERENCES (Continued)

18 Luckey, Jenkins, and Wilson, Phys. Rev. 91, 468 (1953).
G. Bernardini, private communication.

19 Cornelius, Sargent, Rinehart, Lederman, and Rogers, Phys. Rev., in press.

20 G. Cocconi and A. Silverman, Phys. Rev. 88, 1230 (1952).

21 Henley, Ruderman, and Steinberger, Annual Review of Nuclear Science, 1953, to be published.

22 R. H. Hildebrand, Phys. Rev. 89, 1090 (1953).

23 Ajzenberg and Lauritsen, Rev. of Mod. Phys. 24, 321 (1952).

24 L. Van Hove, Phys. Rev. 88, 1358 (1952).

25 The $\pi^+ \rightarrow \pi^+$ phase shifts of Table V differ from those previously reported.[7] This difference is in part due to the difference in relevant energy, but, in Set II particularly, there are additional differences due to the inclusion of the π^- data in the best fit.

26 In a preliminary report of this work, Bul. Am. Phys. Soc., Chicago Meeting 1953, we had not considered this possibility.

27 Byfield, Kessler, and Lederman, Phys. Rev. 86, 17 (1952).

28 H. A. Bethe, Phys. Rev. 90, 994 (1953).

29 Barnes, Angell, Perry, Miller, Ring, and Nelson, preprint of Letter to Editor, Phys. Rev.

30 G. Chew, Phys. Rev. 89, 591 (1953).

31 Bethe, Dyson, Mitra, Ross, Salpeter, Schweber, Sundaresan, and Visscher, Phys. Rev. 90, 372 (1953).

FIGURE CAPTIONS

Fig. 1. Experimental arrangement ($\pi^- + P \rightarrow \pi^- + P$).

Fig. 2. Liquid hydrogen target.

Fig. 3. Liquid scintillation counter used in detection telescope for elastic scattering.

Fig. 4. Y-ray detection telescope used in charge exchange scattering.

Fig. 5. Block diagram of electronics.

Fig. 6. Range curves for positive and negative meson beams.

Fig. 7. Angular resolution in elastic scattering, measured by rotating detecting telescope through forward angles. (For $\pi^+ + P \rightarrow \pi^+ + P$, with L = 27.5 inches.)

Fig. 8. Lateral distribution of positive meson beam directly behind hydrogen target measured with small scanning counter.

Fig. 9. Comparison of experimental cross sections of $\pi^+ \rightarrow \pi^+$ scattering at 58 Mev with results from phase shifts of Sets I and II. Experimental points are given with probable errors.

Fig. 10. Comparison of experimental cross sections of $\pi^- \rightarrow \pi^-$ scattering at 65 Mev with results from phase shifts of Sets I and II. Experimental points are given with probable errors.

FIGURE CAPTIONS (Continued)

Fig. 11. Comparison of observed γ-ray counting rates in $\pi^- \rightarrow \pi^0$ scattering at 65 Mev with results from phase shifts of Sets I and II. The probable errors indicated for the experimental points do not include an over-all uncertainty of $\pm$ 10% in γ-ray efficiency determination.

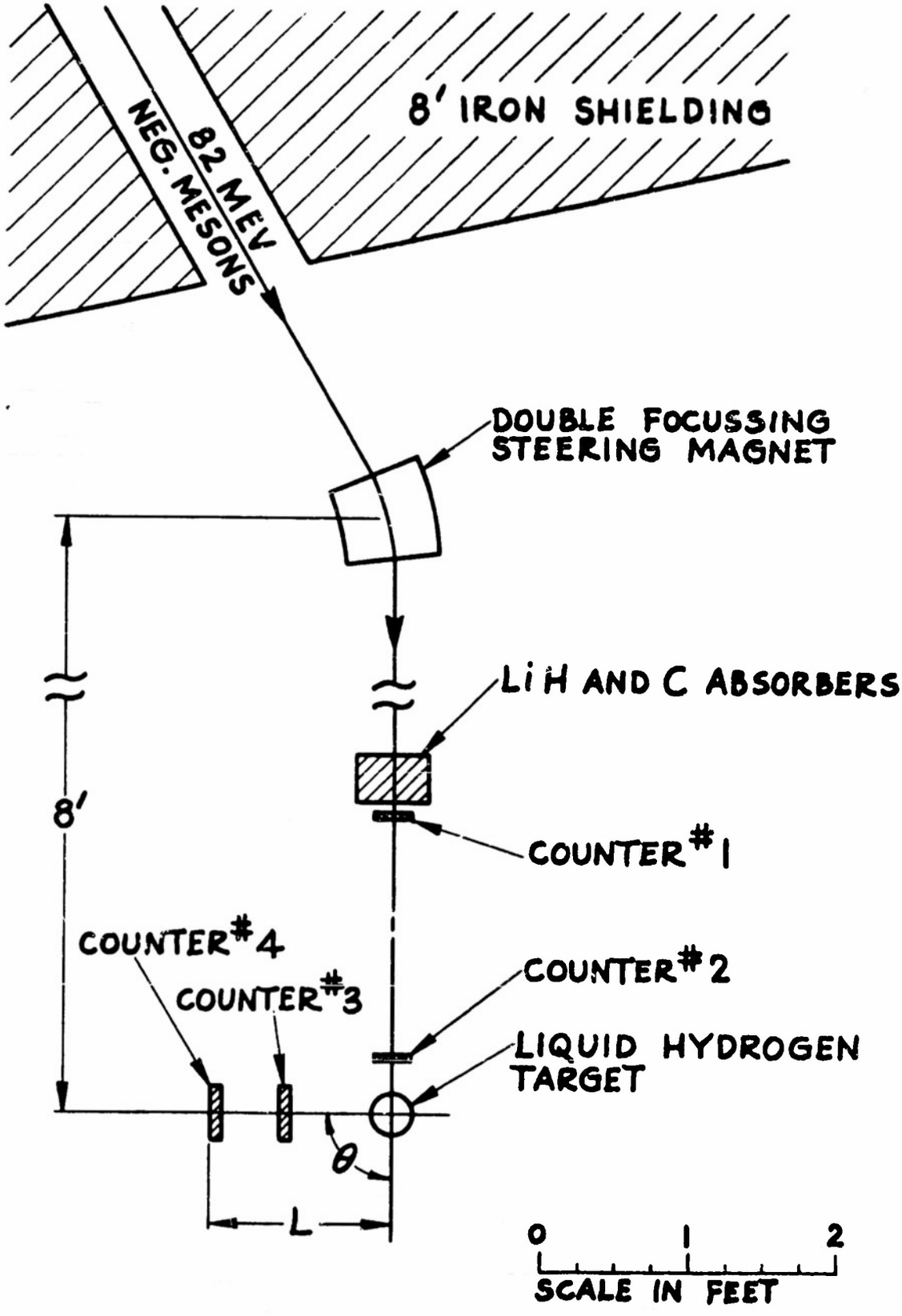
8' IRON SHIELDING
82 MEV
NEG. MESONS
DOUBLE FOCUSSING
STEERING MAGNET
LiH AND C ABSORBERS
COUNTER #1
COUNTER #4
COUNTER #3
COUNTER #2
LIQUID HYDROGEN
TARGET
8'
θ
L
0
1
2
SCALE IN FEET

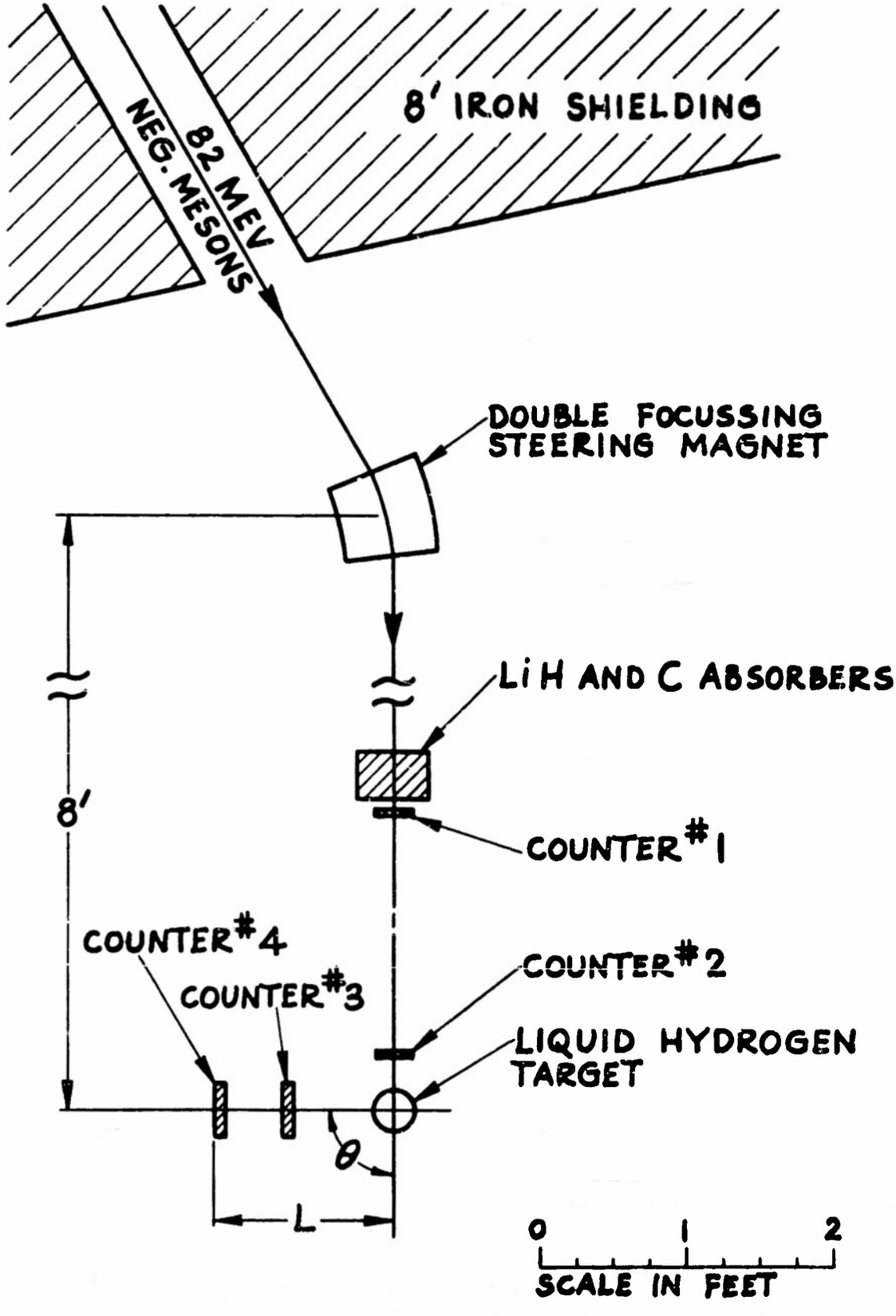
8' IRON SHIELDING
82 MEV
NEG. MESONS
DOUBLE FOCUSSING
STEERING MAGNET
LiH AND C ABSORBERS
8'
COUNTER # 1
COUNTER # 4
COUNTER # 3
COUNTER # 2
LIQUID HYDROGEN
TARGET
θ
L
0
1
2
SCALE IN FEET

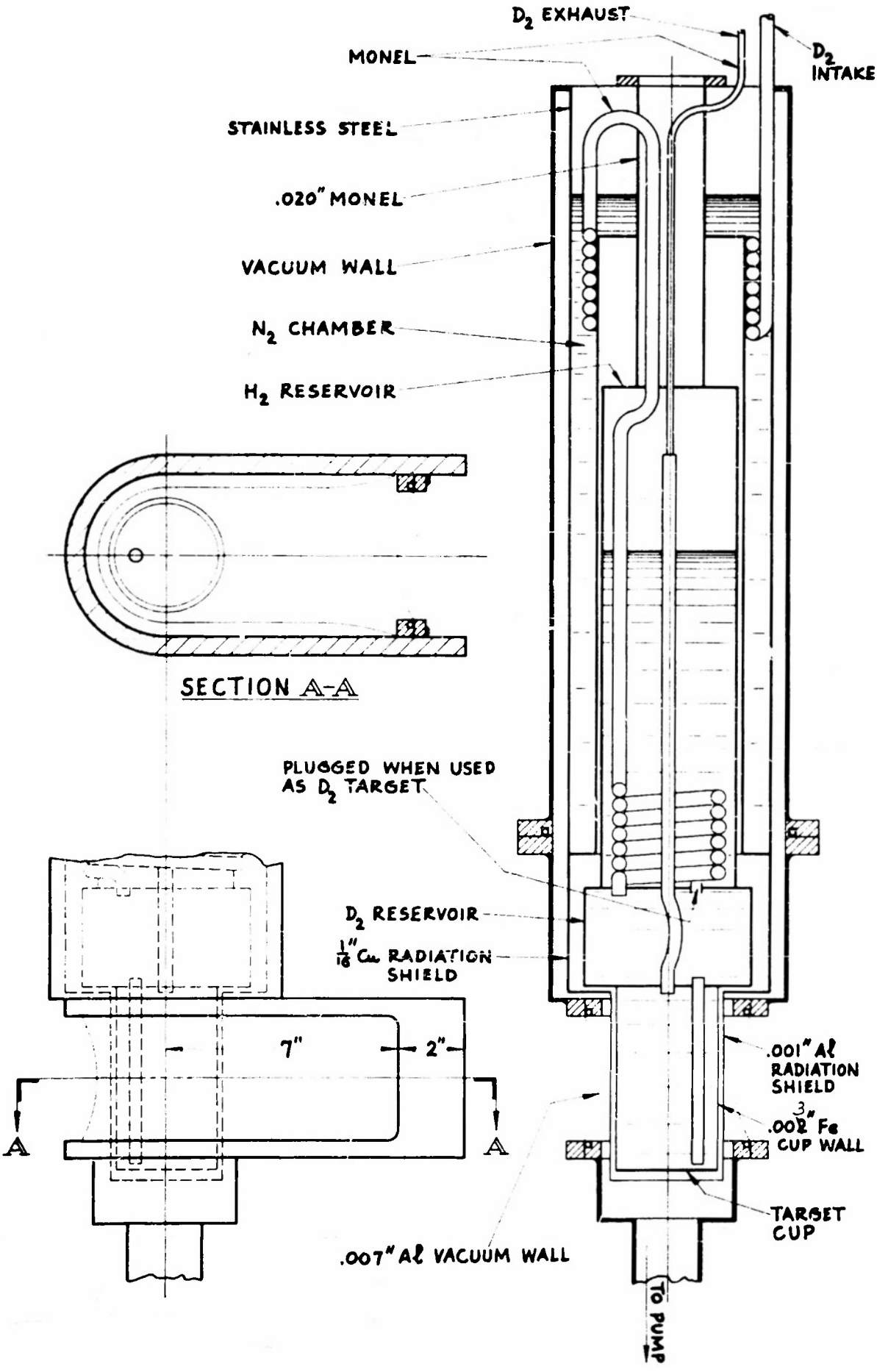
D_2 EXHAUST
MONEL
D_2 INTAKE
STAINLESS STEEL
.020" MONEL
VACUUM WALL
N_2 CHAMBER
H_2 RESERVOIR
SECTION A-A
PLUGGED WHEN USED AS D_2 TARGET
D_2 RESERVOIR
1/16" Cu RADIATION SHIELD
7"
2"
A
A
.001" Al RADIATION SHIELD
3/32" Fe CUP WALL
TARGET CUP
.007" Al VACUUM WALL
TO PUMP

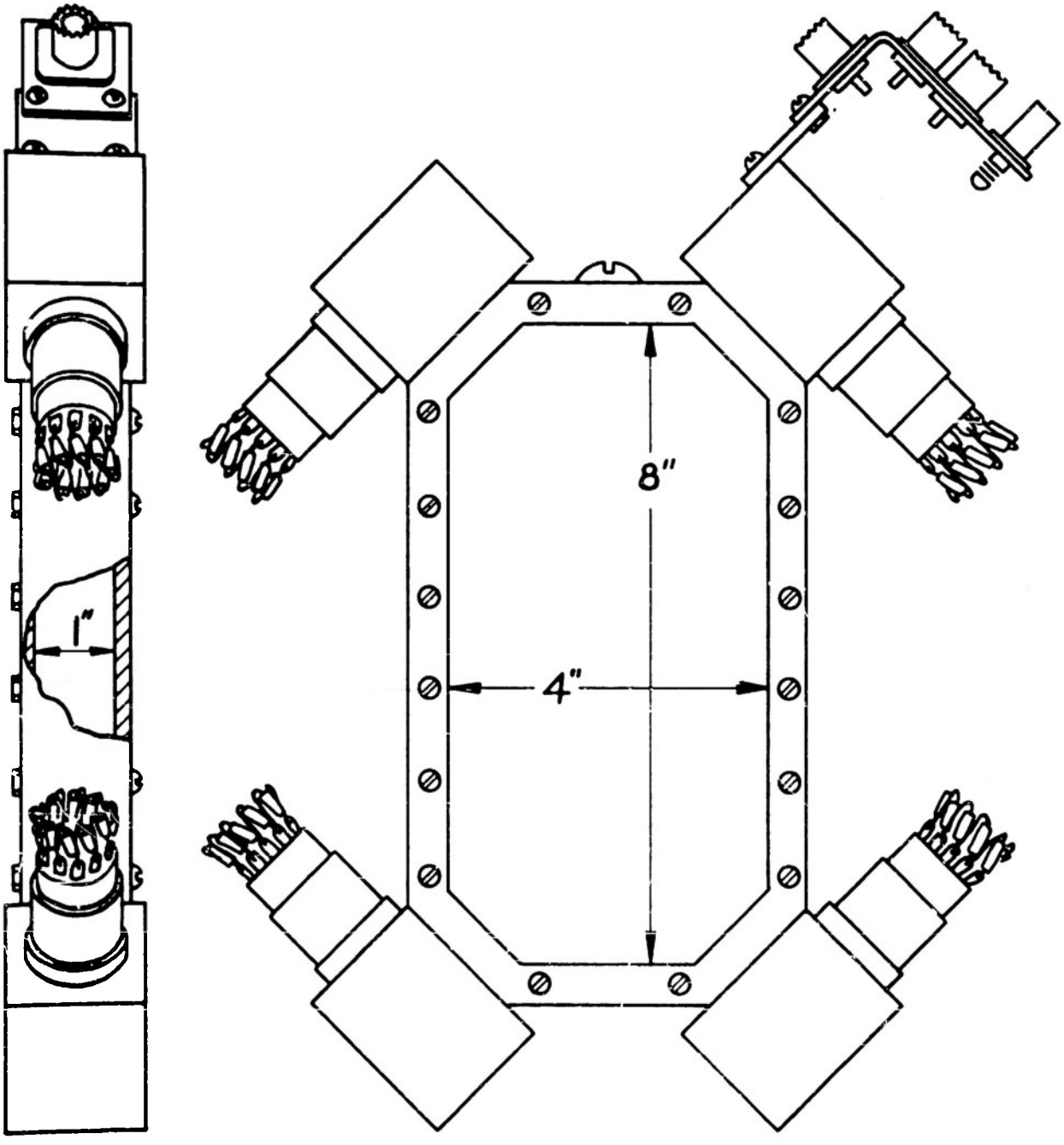
1"
8"
4"

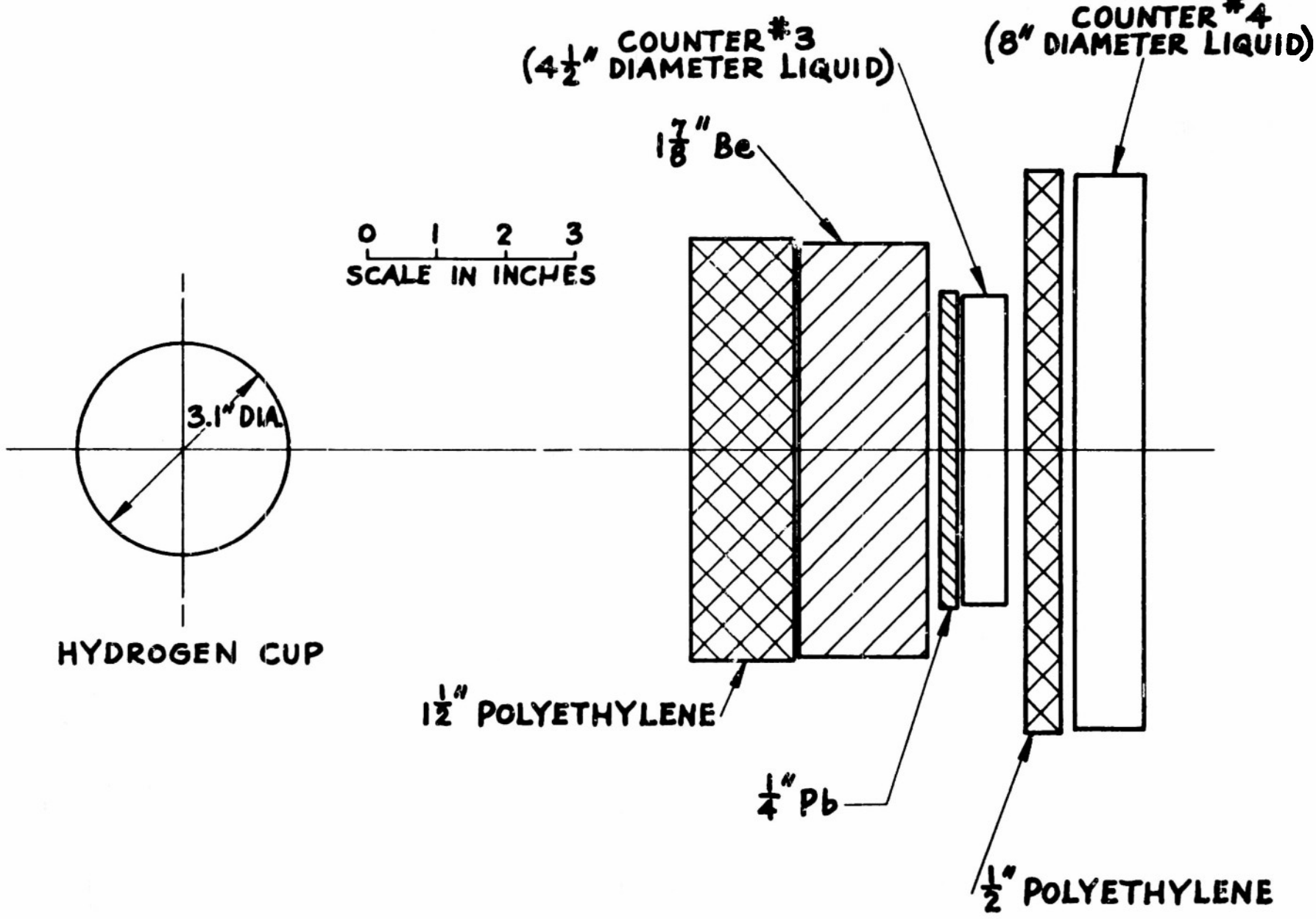
COUNTER #3
(4½" DIAMETER LIQUID)
COUNTER #4
(8" DIAMETER LIQUID)
1⅞" Be
0 1 2 3
SCALE IN INCHES
3.1" DIA.
HYDROGEN CUP
1½" POLYETHYLENE
¼" Pb
½" POLYETHYLENE

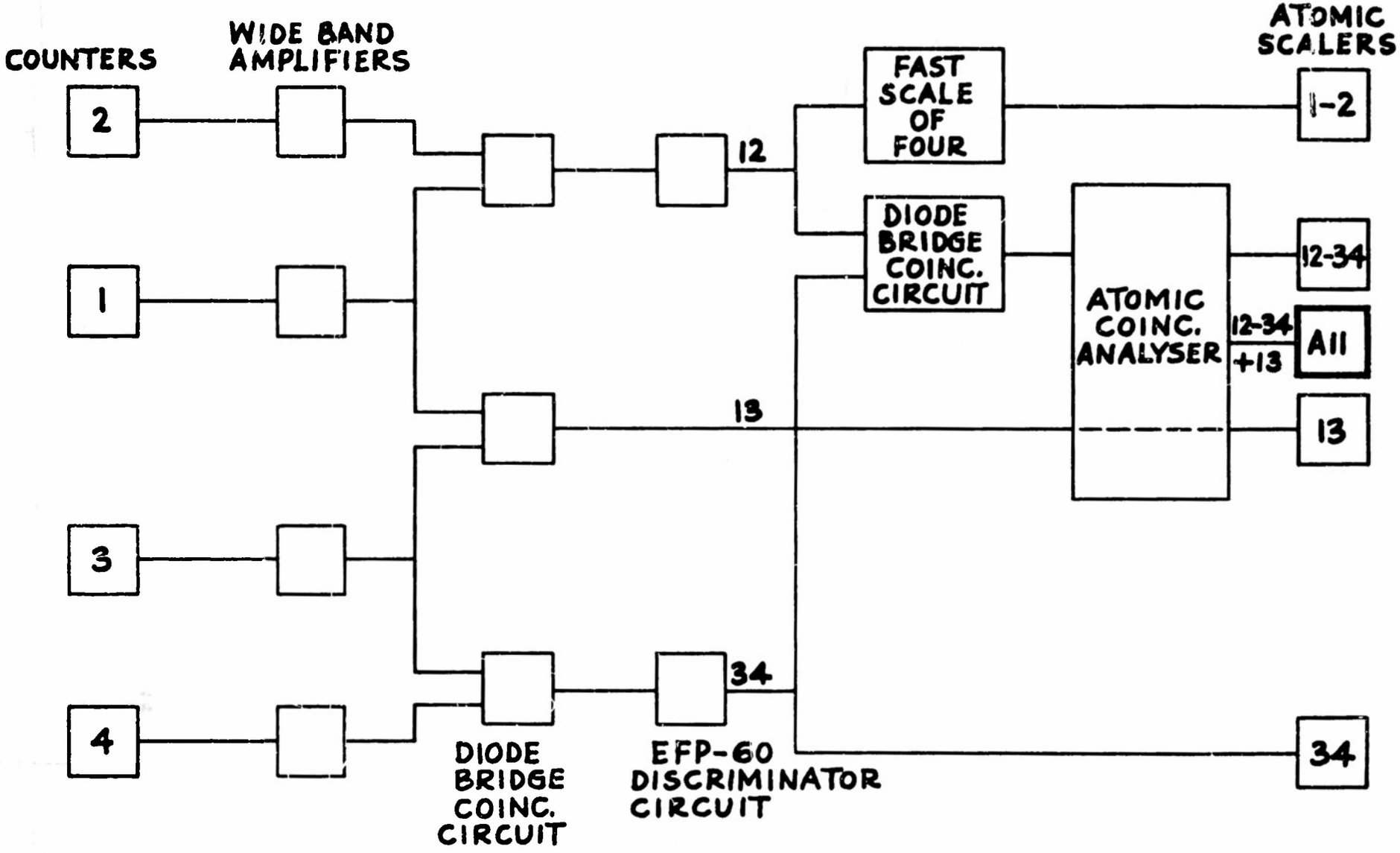
COUNTERS
WIDE BAND AMPLIFIERS
ATOMIC SCALERS
2
1
3
4
12
13
34
FAST SCALE OF FOUR
DIODE BRIDGE COINC. CIRCUIT
ATOMIC COINC. ANALYSER
1-2
12-34
12-34 +13
All
13
34
DIODE BRIDGE COINC. CIRCUIT
EFP-60 DISCRIMINATOR CIRCUIT

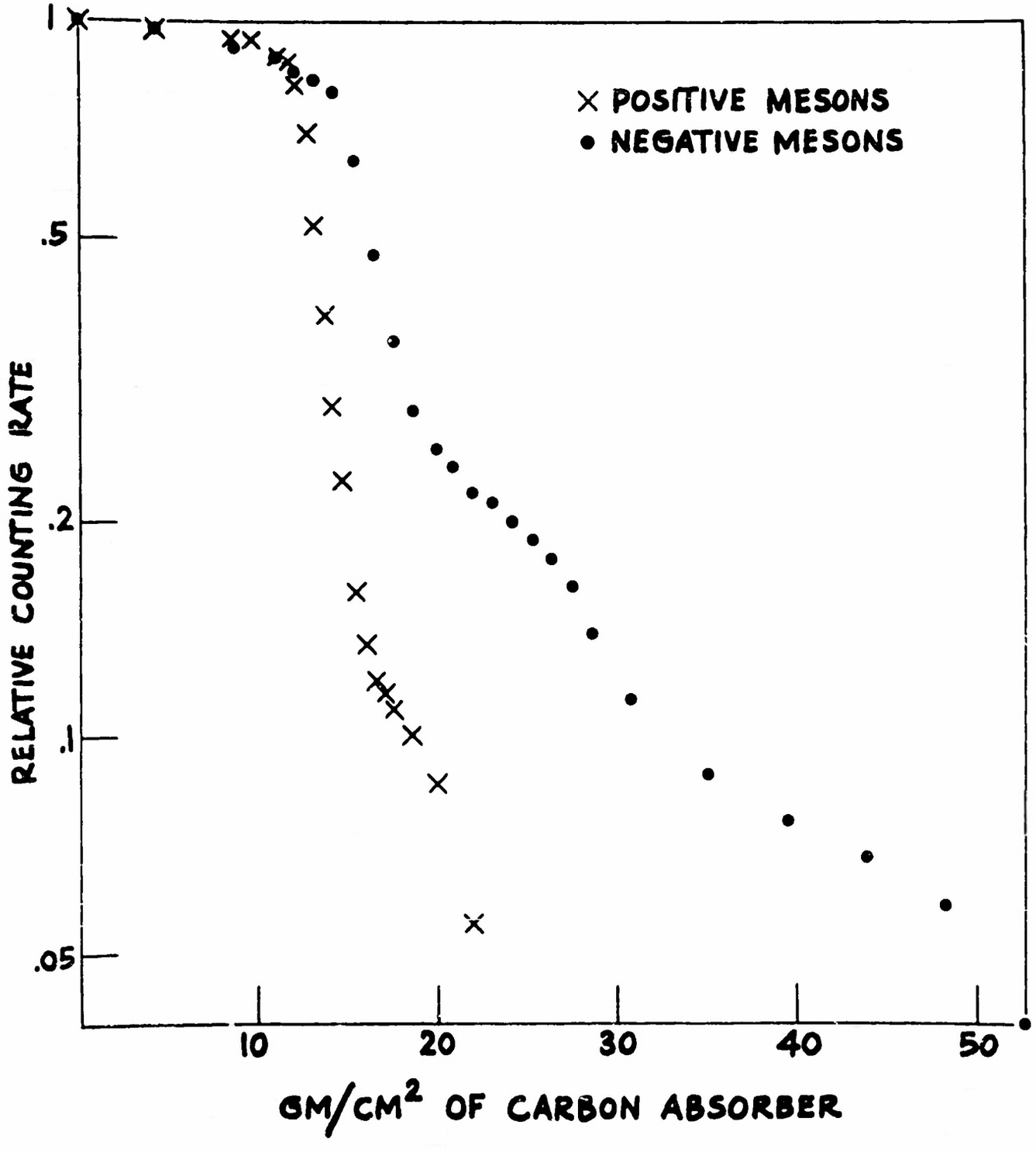
× POSITIVE MESONS
• NEGATIVE MESONS
RELATIVE COUNTING RATE
1
.5
.2
.1
.05
10
20
30
40
50
GM/CM² OF CARBON ABSORBER

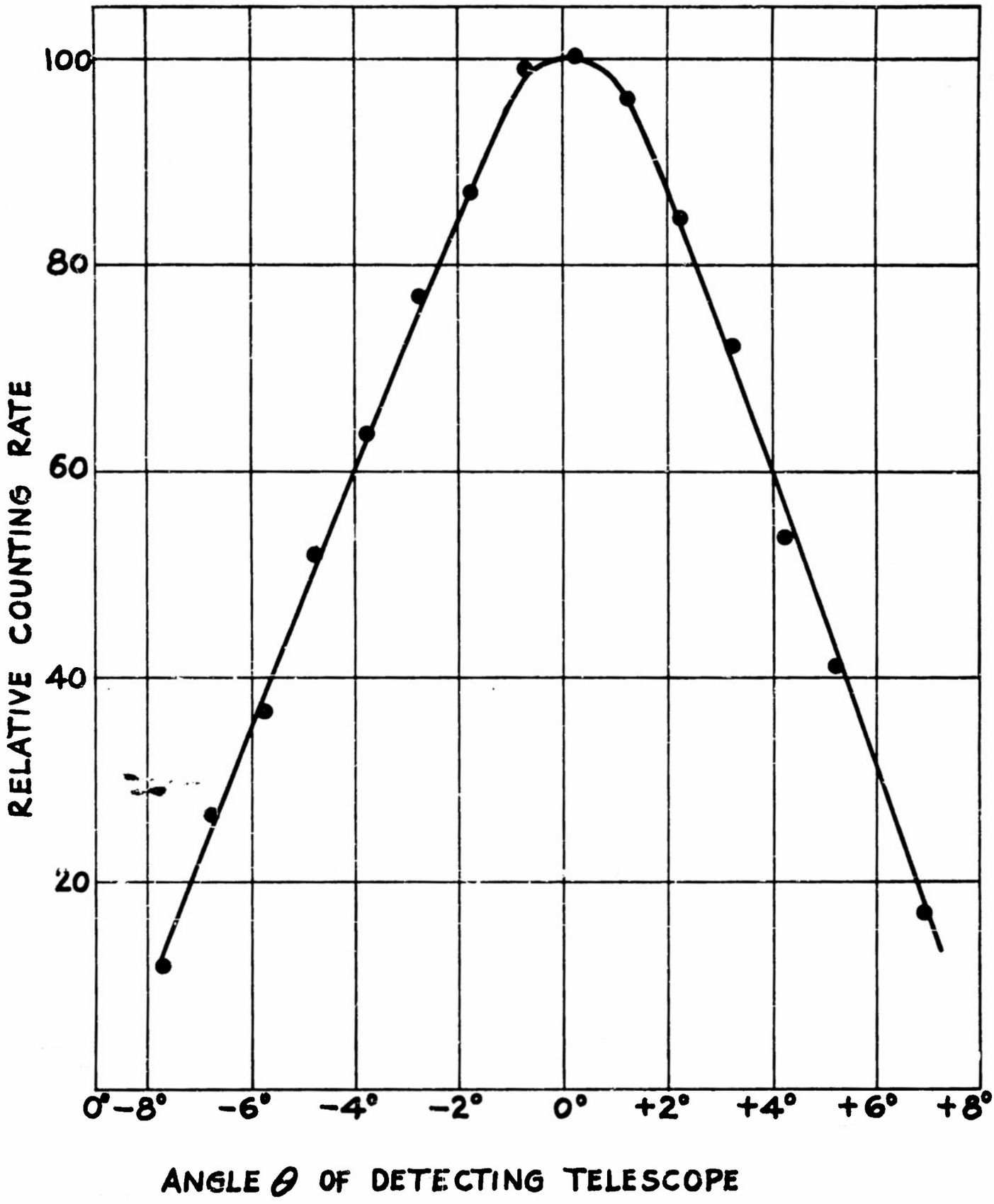
100
80
60
40
20
RELATIVE COUNTING RATE
0°
-8°
-6°
-4°
-2°
0°
+2°
+4°
+6°
+8°
ANGLE θ OF DETECTING TELESCOPE

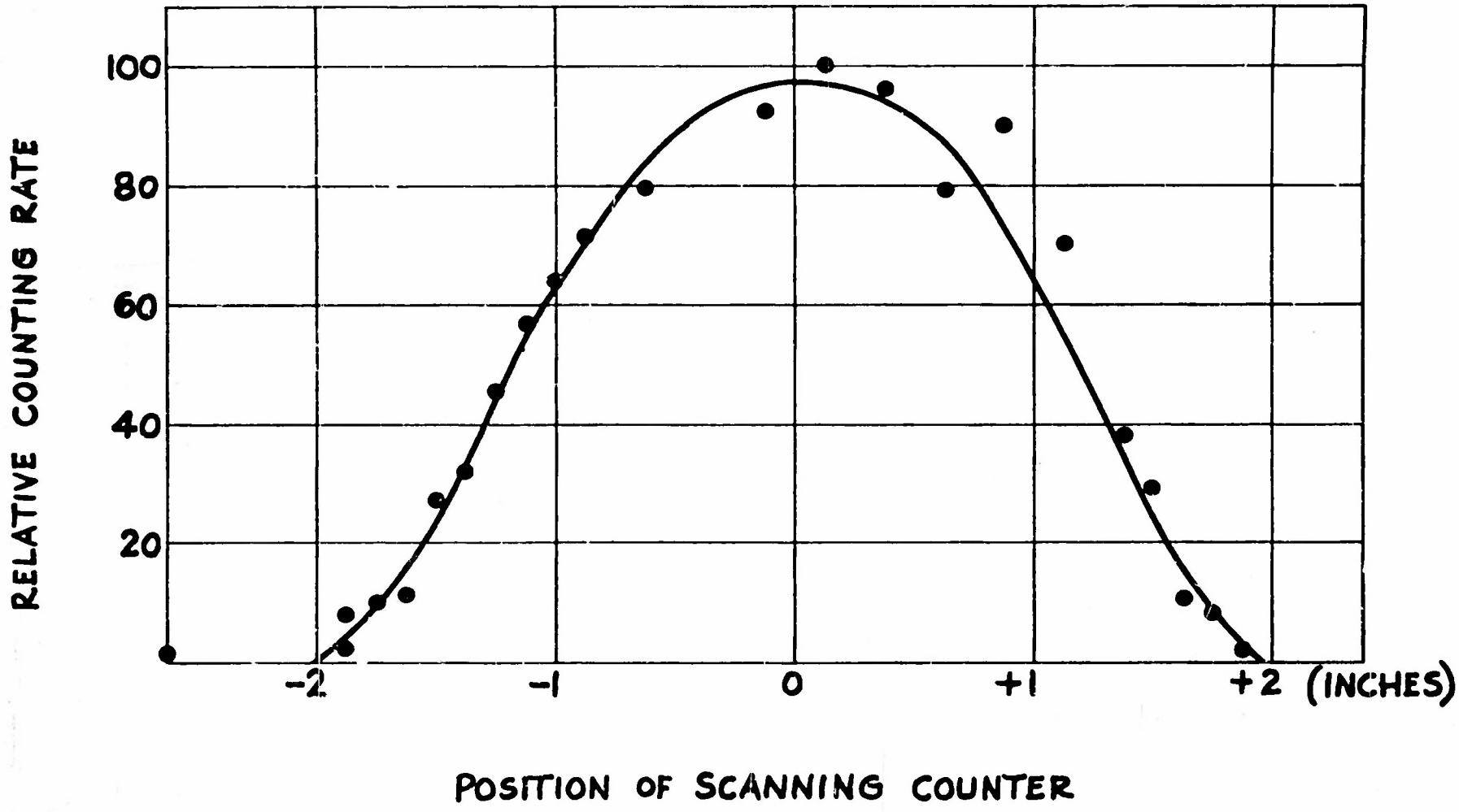
RELATIVE COUNTING RATE
100
80
60
40
20
-2
-1
0
+1
+2
(INCHES)
POSITION OF SCANNING COUNTER

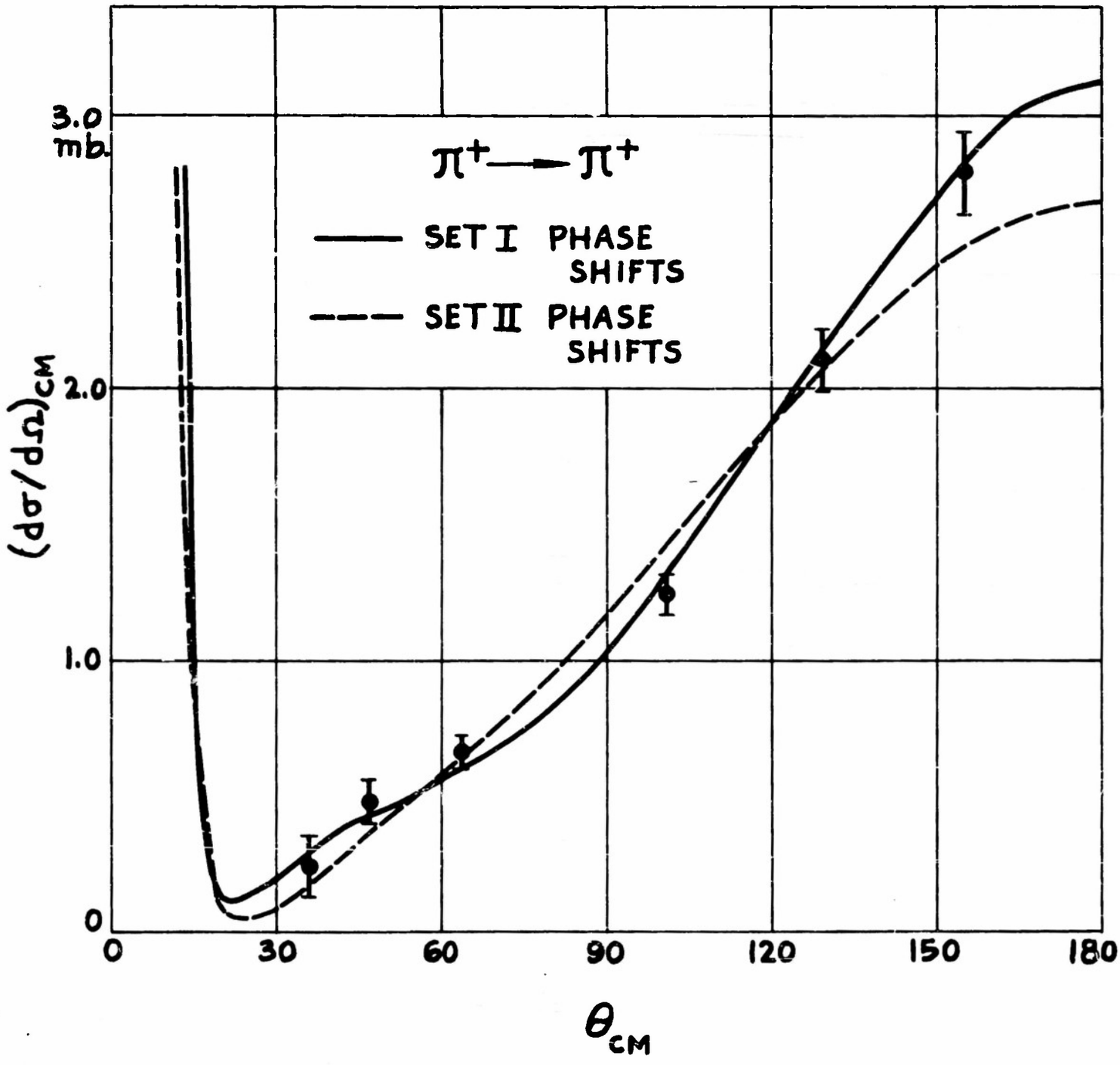
3.0
mb.
2.0
1.0
0
$(d\sigma/d\Omega)_{CM}$
$\pi^+ \longrightarrow \pi^+$
SET I PHASE SHIFTS
SET II PHASE SHIFTS
0
30
60
90
120
150
180
θ_{CM}

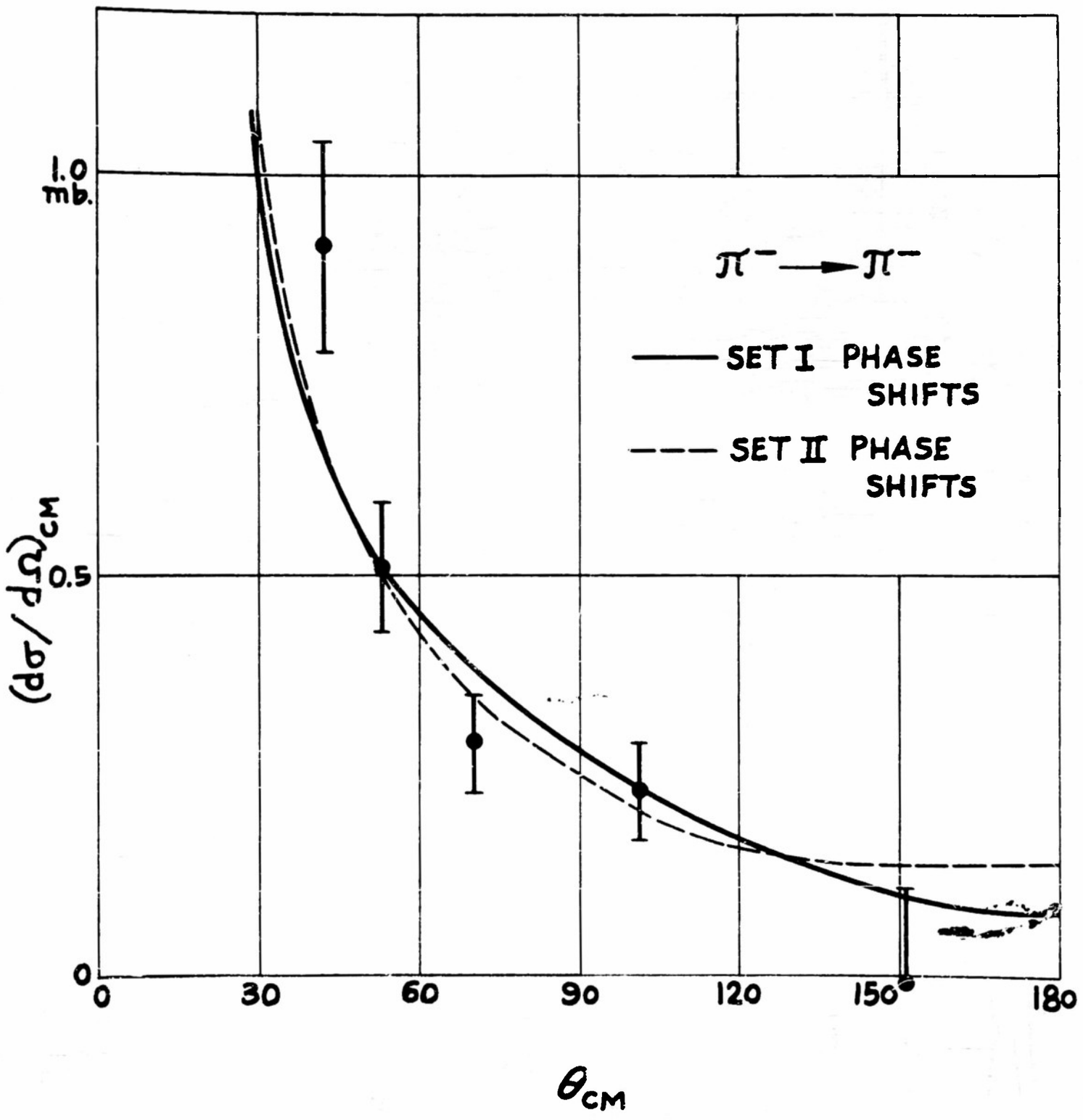
1.0
mb.
0.5
0
$(d\sigma/d\Omega)_{CM}$
$\pi^- \longrightarrow \pi^-$
SET I PHASE SHIFTS
SET II PHASE SHIFTS
0
30
60
90
120
150
180
θ_{CM}

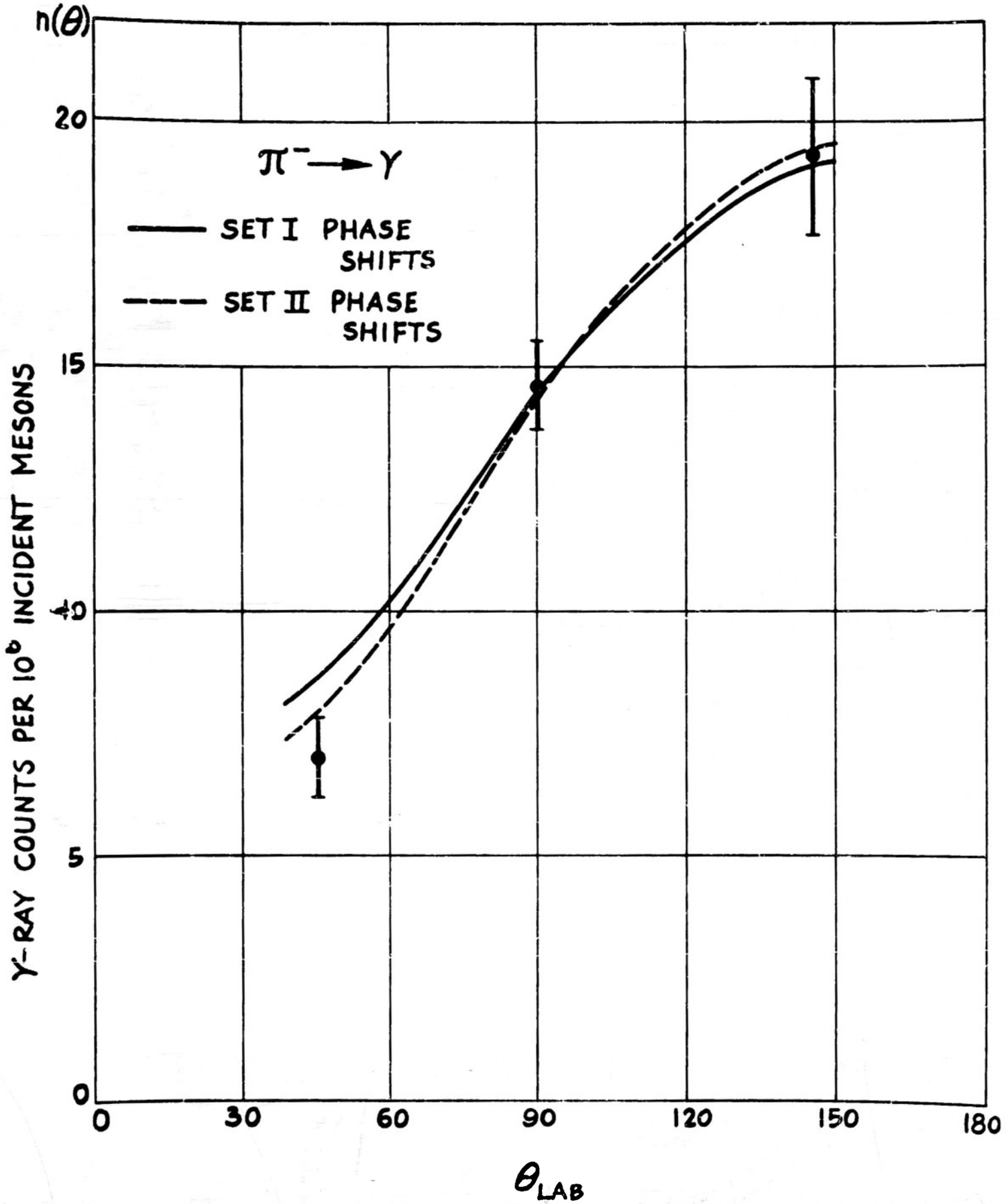
n(θ)
20
15
10
5
0
π⁻ → γ
SET I PHASE SHIFTS
SET II PHASE SHIFTS
γ-RAY COUNTS PER 10⁶ INCIDENT MESONS
0
30
60
90
120
150
180
θLAB

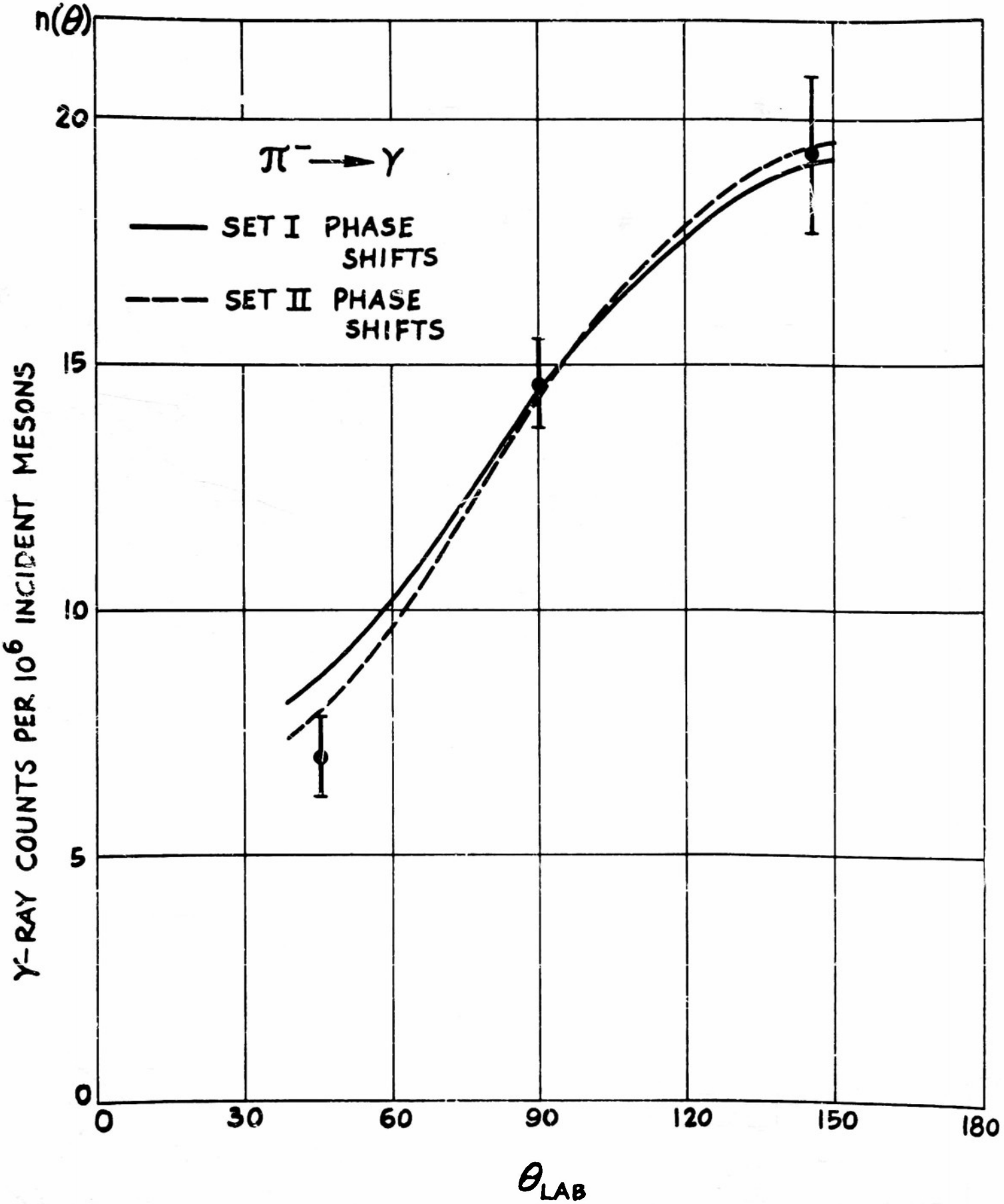
n(θ)
20
15
10
5
0
π⁻ → γ
SET I PHASE SHIFTS
SET II PHASE SHIFTS
Y-RAY COUNTS PER 10⁶ INCIDENT MESONS
0
30
60
90
120
150
180
θLAB